AAS 16-236

PROBABILISTIC INITIAL ORBIT DETERMINATION

Roberto Armellin[*], Pierluigi Di Lizia[†]

Future space surveillance requires dealing with uncertainties directly in the initial orbit determination phase. We propose an approach based on Taylor differential algebra to both solve the initial orbit determination (IOD) problem and to map uncertainties from the observables space into the orbital elements space. This is achieved by approximating in Taylor series the general formula for pdf mapping through nonlinear transformations. In this way the mapping is obtained in an elegant and general fashion. The proposed approach is applied to both angles-only and two position vectors IOD for objects in LEO and GEO.

INTRODUCTION

The total number of active satellites, rocket bodies, and debris larger than 10 cm is currently about 20,000. Considering all resident space objects larger than 1 cm this rises to an estimated minimum of 500,000 objects. Latest generation sensor networks will produce millions of observations per day. Identifying observations belonging to the same object will be one of the main challenges of orbit determination. One requirement to perform reliable data association is to have realistic uncertainties for initial orbit solutions, which also allows one to initialize Bayesian estimators for orbit refinement.[1] In order to meet this requirement two main steps are required: solve the initial orbit determination (IOD) problem, and map the error distributions from observations to the initial orbit solutions. Addressing the second requirement is the main focus of this work.

In IOD the number of observations is equal to the number of unknowns, and thus a nonlinear system of equations needs to be solved. In IOD simplified dynamical models are often used (e.g. Keplerian motion) and measurement errors are not taken into account (the problem is deterministic). Based on the set of available measurements, a different IOD problem can be framed. In this work we consider two cases: angles-only and two position vectors IOD. In angles-only IOD a resident space object (RSO) is observed three times with optical sensors on a single passage. Angles-only IOD is an old problem. Gauss'[2] and Laplace's[3] methods are commonly used to determine a Keplerian orbit that fits with three astrometric observations. These methods have been revisited and analyzed by a large number of authors,[4,5,6] and new ones introduced more recently. The Double r-iteration technique of Escobal[7] and the approach of Gooding[8] are two examples of angles-only methods introduced for the IOD of RSO. In the two position vectors problem, two range measurements are obtained with a radar together with the information on instrument pointing angles. In this case the classical Lambert's problem can be formulated.[9] Although this problem was solved more

[*] IEF Marie Sklodowska-Curie Fellow, Departamento de Matemáticas y Computación, Universidad de La Rioja, 26006 Logrono, Spain (roberto.armellin@unirioja.es)

[†] Assistant Professor, Department of Aerospace Science and Technology, Politecnico di Milano, 20156 Milan, Italy (pierluigi.dilizia@polimi.t)

than 200 years ago, many researchers are still working on devising robust and efficient resolution procedures.[10,11]

In general, the solution of both angles-only and two position vectors IOD is numerical and thus an explicit function that relates the observations with the object orbital parameters is not available. As a result, the methods proposed in the literature to map observation statistics into initial orbit statistics rely either on linearizations[12] or particle-based algorithms.[13,14,15] In this work we approximate the IOD implicit relations as explicit high order Taylor polynomials in the observations, by using differential algebra (DA).[16] DA is used to solve the nonlinear equations associated to the IOD problem as well as to expand the solution in Taylor series with respect to measurement variables. We refer to this map as the observations-to-solution (O2S) map. This approximation can be suitably used to map samples from the observation space into the RSO orbital parameters space, thus enabling for example efficient Monte Carlo simulations. More importantly the O2S polynomial (and the Taylor representation of its inverse, the S2O map) allows us to analytically represent the pdf of the IOD solution for any arbitrary pdf of the measurements. This is simply achieved by expanding in Taylor series also the determinant of the Jacobian of the O2S map and using well known formula for pdf transformation.[17,18] This approach is independent on the representation of the dynamics and thus the Keplerian approximation can be removed.

The paper is organised as follows. An introduction on DA is given first together with the algorithms for the expansion of the solution of implicit equations and the solution of a system of ODE. The section after describes in a general fashion how DA can be used for pdf mapping, using the cartesian to polar transformation as an illustrative example. This method is then detailed for the specific application to angles-only and two position vectors IOD. The optical observation of GEO spacecraft and the radar observation of an RSO in LEO are used as test cases to discuss the method's features and performance. Some final remarks conclude the paper.

DIFFERENTIAL ALGEBRA TOOLS

DA supplies the tools to compute the derivatives of functions within a computer environment.[16] More specifically, by substituting the classical implementation of real algebra with the implementation of a new algebra of Taylor polynomials, any function f of v variables is expanded into its Taylor polynomial up to an arbitrary order k with limited computational effort. In addition to basic algebraic operations, operations for differentiation and integration can be easily introduced in the algebra, thusly finalizing the definition of the differential algebra structure of DA.[19,20] Similarly to algorithms for floating point arithmetic, various algorithms were introduced in DA, including methods to perform composition of functions, to invert them, to solve nonlinear systems explicitly, and to treat common elementary functions.[21] The DA used for the computations in this work was implemented in the software COSY INFINITY.[22] The reader may refer to[23] for the DA notation adopted throughout the paper.

High-order expansion of the solution of ODE

An important application of DA is the automatic high order expansion of the solution of an ODE in terms of the initial conditions.[21,23] This can be achieved by replacing the operations in a classical numerical integration scheme, including evaluation of the right hand side, by the corresponding DA operations. This way, starting from the DA representation of an initial condition x_0, DA-based ODE integration allows the propagation of the Taylor expansion of the flow in x_0 forward in time, up to any final time t_f. Any explicit ODE integration scheme can be rewritten as a DA integration scheme

in a straightforward way. For the numerical integrations presented in this paper, a DA version of a 7/8 Dormand-Prince (8-th order solution for propagation, 7-th order solution for step size control) Runge-Kutta scheme is used. The main advantage of the DA-based approach is that there is no need to write and integrate variational equations in order to obtain high order expansions of the flow. It is therefore independent of the particular right hand side of the ODE and the method is quite efficient in terms of computational cost.

Expansion of the solution of parametric implicit equations

Well-established numerical techniques (e.g., Newton's method) exist to compute numerically the solution of an implicit equation

$$\boldsymbol{h}(\boldsymbol{y}) = 0, \tag{1}$$

with $\boldsymbol{h} : \Re^n \to \Re^n$. Suppose an explicit dependence on a vector of parameters $\boldsymbol{x}$ can be highlighted in the vector function $\boldsymbol{h}$, which leads to the parametric implicit equation

$$\boldsymbol{h}(\boldsymbol{y}, \boldsymbol{x}) = 0. \tag{2}$$

We look for the function $\boldsymbol{y} = \boldsymbol{f}(\boldsymbol{x})$ that solves (2) for any value of $\boldsymbol{x}$.

DA techniques can effectively handle the previous problem by representing $\boldsymbol{f}(\boldsymbol{x})$ in terms of its Taylor expansion with respect to $\boldsymbol{x}$. This result is achieved by applying partial inversion techniques as detailed in Di Lizia et al.[23] The final result is

$$\boldsymbol{y} = \mathcal{T}^k_{\boldsymbol{f}(\boldsymbol{x})}(\boldsymbol{x}), \tag{3}$$

which is the k-th order Taylor expansion of the solution of the implicit equation. For every value of $\boldsymbol{x}$, the approximate solution of $\boldsymbol{h}(\boldsymbol{y}, \boldsymbol{x}) = 0$ can be easily computed by evaluating the Taylor polynomial (3). Apparently, the solution obtained by means of the polynomial map (3) is a Taylor approximation of the exact solution of Eq. (2). The accuracy of the approximation depends on both the order of the Taylor expansion and the displacement $\delta\boldsymbol{x}$ from the reference value of the parameter.

IOD problems can be framed as (2), in which the vector of parameters $\boldsymbol{x}$ represents the observations, $\boldsymbol{y}$ is spacecraft state, and $\boldsymbol{h}(\boldsymbol{y}, \boldsymbol{x})$ is the function of the defects. Within this framework Eq. (3) is a Taylor polynomial that relates a variation in the observation vector to a variation in object state, i.e. the O2S map.

DA-BASED PDF MAPPING

We are given two n-dimensional random vectors $\boldsymbol{x}$ and $\boldsymbol{y}$, related by continuous one-to-one transformations $\boldsymbol{y} = \boldsymbol{f}(\boldsymbol{x})$ and $\boldsymbol{x} = \boldsymbol{g}(\boldsymbol{y})$, and the probability density function $p(\boldsymbol{x})$. Using the axiom of probability conservation and the rules of change of variables in multiple integrals, the probability density function of $\boldsymbol{y}$ can be written as[17]

$$p(\boldsymbol{y}) = p(\boldsymbol{g}(\boldsymbol{y})) \left| \det \frac{\partial \boldsymbol{g}}{\partial \boldsymbol{y}} \right|, \tag{4}$$

in which det indicated the determinant. By substitution, the expression (4) can be rewritten in terms of the original variables $\boldsymbol{x}$ as

$$p(\boldsymbol{f}(\boldsymbol{x})) = p(\boldsymbol{x}) \; 1 \Big/ \left| \det \frac{\partial \boldsymbol{f}}{\partial \boldsymbol{x}} \right|. \tag{5}$$

The problem that we want to address here is mapping the pdf of the observations into the pdf of the orbital parameters. Within this framework the observation set is represented by the vector $\boldsymbol{x}$ with known $p(\boldsymbol{x})$. In IOD we typically do not have the explicit relation between the observations into the orbital parameters, i.e. $\boldsymbol{y} = \boldsymbol{f}(\boldsymbol{x})$, but only an implicit relation in the form $\boldsymbol{h}(\boldsymbol{y}, \boldsymbol{x}) = 0$. For this reason it is in practice difficult to obtain an analytical expression of the mapped pdf.

As explained in Section *Expansion of the solution of parametric implicit equations*, with DA a polynomial representation of the S2O map, i.e. (3), can be obtained. This relation can also be inverted delivering the Taylor approximation of the O2S map

$$\boldsymbol{x} = \mathcal{T}_{\boldsymbol{g}(\boldsymbol{y})}(\boldsymbol{y}), \tag{6}$$

in which the superscript k has been omitted for the sake of a lighter notation.

Furthermore, the Taylor approximations of the determinant of the Jacobian of both the direct and inverse relations can be easily obtained. The computation of (5) and (4) can be then carried out in DA as

$$p(\boldsymbol{y}) = p\left(\mathcal{T}_{\boldsymbol{g}(\boldsymbol{y})}(\boldsymbol{y})\right) \mathcal{T}_{\left|\det \frac{\partial \boldsymbol{g}}{\partial \boldsymbol{y}}\right|}(\boldsymbol{y}) \tag{7}$$

and

$$p\left(\mathcal{T}_{\boldsymbol{f}(\boldsymbol{x})}(\boldsymbol{x})\right) = p\left(\boldsymbol{x}\right)\ 1 \Big/ \mathcal{T}_{\left|\det \frac{\partial \boldsymbol{f}}{\partial \boldsymbol{x}}\right|}(\boldsymbol{x}). \tag{8}$$

This approach will be labeled as partial DA mapping method as in both equations (7) and (8) the final pdf is obtained by the multiplication of the starting pdf with a Taylor polynomial. In the full DA mapping, instead, also $p(\boldsymbol{x})$ is approximated as a Taylor polynomial, thus delivering a full polynomial representation of the mapped pdf. Note that, in the latter approach, as $p(\boldsymbol{x})$ is an asymptotic function, the accuracy of its Taylor representation will be limited even when the computations are carried out at high orders.

Example: cartesian to polar transformation

In this section we use for illustrative purposes the problem of mapping a Gaussian pdf from cartesian to polar coordinates. The cartesian to polar coordinate transformation is given by

$$\boldsymbol{y} = \boldsymbol{f}(\boldsymbol{x}) = \begin{pmatrix} \sqrt{x_1^2 + x_2^2} \\ \operatorname{atan} \frac{x_2}{x_1} \end{pmatrix} \tag{9}$$

and we assume that $\boldsymbol{x}$ is a Gaussian random vector (GRV), $p(\boldsymbol{x}) = \mathcal{N}(\boldsymbol{\mu}, \boldsymbol{P})$, in which $\boldsymbol{\mu} = (\mu_1, \mu_2)$ is the mean vector and $\boldsymbol{P}$ is a diagonal covariance matrix defined by the standard deviations σ_1 and σ_2. The goal is to compute the mapped pdf $p(\boldsymbol{y})$.

In this simple case we can compute the solution analytically. To write (4), we compute the inverse transformation

$$\boldsymbol{x} = \boldsymbol{g}(\boldsymbol{y}) = \begin{pmatrix} y_1 \cos y_2 \\ y_1 \sin y_2 \end{pmatrix} \tag{10}$$

and the determinant of its Jacobian

$$\left|\det\frac{\partial \boldsymbol{g}}{\partial \boldsymbol{y}}\right| = y_1. \tag{11}$$

The mapped pdf can be written as

$$p(\boldsymbol{y}) = \mathcal{N}(\boldsymbol{\mu}, \boldsymbol{P})y_1 \tag{12}$$

leading to

$$p(\boldsymbol{y}) = \frac{\exp\left(-\frac{(y_1\cos(y_2)-\mu_1)^2}{2\sigma_1^2} - \frac{(y_1\sin(y_2)-\mu_2)^2}{2\sigma_2^2}\right) y_1}{2\pi\sigma_1\sigma_2}. \tag{13}$$

To avoid the computation of the inverse transformation we can use the expression (5), which in this case reads

$$p(\boldsymbol{y}) = p(\boldsymbol{f}(\boldsymbol{x})) = \mathcal{N}(\boldsymbol{\mu}, \boldsymbol{P})\sqrt{x_1^2 + x_2^2}; \tag{14}$$

where we have used

$$1\Big/\left|\det\frac{\partial \boldsymbol{f}}{\partial \boldsymbol{x}}\right| = \sqrt{x_1^2 + x_2^2}. \tag{15}$$

Explicitly we have

$$p(\boldsymbol{y}) = p(\boldsymbol{f}(\boldsymbol{x})) = \frac{\exp\left(-\frac{(x_1-\mu_1)^2}{2\sigma_1^2} - \frac{(x_2-\mu_2)^2}{2\sigma_2^2}\right)\sqrt{x_1^2 + x_2^2}}{2\pi\sigma_1\sigma_2}. \tag{16}$$

Figure 1(a) shows the contour levels for $\boldsymbol{\mu} = (5, 4)$ and $\boldsymbol{\sigma} = (1, 1)$, in the range $\boldsymbol{x} \in \boldsymbol{\mu} \pm \frac{3}{2}\boldsymbol{\sigma}$. In Figure 1(b) the contour levels of the mapped pdf are plotted using the analytical expressions (9) and (16).

In the partial DA method we initialize the state $\boldsymbol{x}$ as DA variable and we compute the Taylor approximation of (9) and (15). Then, for each point $\boldsymbol{x} \in \boldsymbol{\mu} \pm \frac{3}{2}\boldsymbol{\sigma}$, we compute the approximated values of both $\boldsymbol{y}$ and the inverse of the determinant of the Jacobian. The contour levels of $1\Big/\mathcal{T}_{\left|\det\frac{\partial \boldsymbol{f}}{\partial \boldsymbol{x}}\right|}(\boldsymbol{x})$ are plotted in Figure 1(c), whereas Figure 1(d) shows the relative errors of the Taylor approximation with respect to the analytical solution. At order 9 the maximum error of the Taylor representation in the considered region is of the order of $1 \times 10^{-3}\%$. The computation of the mapped pdf requires only the multiplication by $p(\boldsymbol{x})$, and the result is shown in Figure 1(e). Clearly the relative error of the mapped pdf is equal to that of the Taylor representation of the the inverse of the determinant of the Jacobian of the transformation, as shown in Figure 1(f). Figure 1(g) shows the contour levels of the mapped pdf obtained with the full DA method, i.e. when also $p(\boldsymbol{x})$ is approximated as a Taylor polynomial. The error of the mapped pdf in this case is a combination of the error of the Taylor approximations of both $p(\boldsymbol{x})$ and the inverse of the determinant of the Jacobian. However, Figure 1(h)

clearly shows that the error on the polynomial representation of $p(\boldsymbol{x})$ prevails: the overall relative errors become large when the probability gets small because the Taylor expansion fails to represent the asymptotic behaviour of $p(\boldsymbol{x})$ independently of the order used.

ANGLES-ONLY IOD

In the classical angles-only IOD problem, three optical observations at epoch t_i, with $i = 1, \ldots, 3$ are available. The observations consist in three couples of right ascension and declination angles, (α_i, δ_i) or with a more compact notation $(\boldsymbol{\alpha}, \boldsymbol{\delta})$. These observations provide us with three inertial light of sights $\hat{\boldsymbol{\rho}}_i$, i.e. the unit vectors pointing from the observer (on the Earth's surface) to the observed object. Taylor DA can be used to solve and expand the solution of the IOD (see Armellin et al.[24]) allowing us to represent the spacecraft state at the epoch of the second observation as Taylor polynomial $\boldsymbol{y}_2 = \mathcal{T}_{\boldsymbol{y}_2}(\boldsymbol{\alpha}, \boldsymbol{\delta})$. This Taylor polynomial is the approximation of the O2S map that tells us how a change in the observation is reflected in a variation of the spacecraft state. If the pdf of the observations, i.e. $p(\boldsymbol{\alpha}, \boldsymbol{\delta})$, is known the DA method for mapping the pdf can be used to estimate spacecraft state pdf at epoch t_2. Note that the solution $\boldsymbol{y}_2$ can be represented in any arbitrary set of orbital parameters. To this aim, the coordinate transformations are included in $\boldsymbol{f}$ in Eq. (5). Consequently, the evaluation of $\boldsymbol{f}$ in the DA framework allows us to obtain the Taylor expansion of the coordinate transformations along with the expansion of the orbital parameters with respect to the observables. Moreover, the pdf can be mapped to any epoch t if the solution of the ODE at t is expanded in Taylor series as explained in Section *High-order expansion of the solution of ODE*. The only requirement is that the Taylor approximations are sufficiently accurate. For a given demanded accuracy, the Taylor expansions radius of convergence can be automatically estimated as explained in Wittig et al.[25]

TWO POSITION VECTORS IOD

In the case of radar observations, two measurements at epoch t_i, with $i = 1, 2$, are available. Each observation consists in the pointing angles (α_i, δ_i) and the range ρ_i, or in a more compact form $(\boldsymbol{\alpha}, \boldsymbol{\delta}, \boldsymbol{\rho})$. By assuming the observer's location as known, a radar observation is equivalent to a measure of the spacecraft position vector. The two position vectors can be approximated in the DA framework as $\boldsymbol{r}_i = \mathcal{T}_{\boldsymbol{r}_i}(\rho_i, \alpha_i, \delta_i)$. With the two position vectors and the elapsed time between the observations, we can formulate a Lambert's problem, which delivers the Taylor approximation of the velocity vectors at the end points when it is solved in the DA framework,[26] i.e. $\boldsymbol{v}_i = \mathcal{T}_{\boldsymbol{v}_i}(\boldsymbol{\alpha}, \boldsymbol{\delta}, \boldsymbol{\rho})$. Note that in this expression $(\boldsymbol{\alpha}, \boldsymbol{\delta}, \boldsymbol{\rho})$ are deviations from the nominal observations. The state of the spacecraft at the epoch of the first observation can then be fully written as a Taylor polynomial $\boldsymbol{y}_1 = \mathcal{T}_{\boldsymbol{y}_1}(\boldsymbol{\alpha}, \boldsymbol{\delta}, \boldsymbol{\rho})$. If the pdf of the observations is known, i.e. $p(\boldsymbol{\alpha}, \boldsymbol{\delta}, \boldsymbol{\rho})$, the DA method for mapping the pdf can be used to estimate initial state pdf. As for the angles-only case, the resulting state can be represented in any coordinate system and/or set of orbital elements, and at any time by suitably expanding in Taylor series the required transformations.

TEST CASES

Single-pass optical and radar observations of the two objects listed in Table 1 are considered as test cases for the pdf mapping based on DA. The first one is INTELSAT 901, a GEO communications spacecraft. The second one is a SL-8 rocket body in LEO.

99.457600000000000e+00 For the object in GEO an optical campaign is simulated with three observations taken with the European Space Agency Optical Ground Station (OGS, Teide Observa-

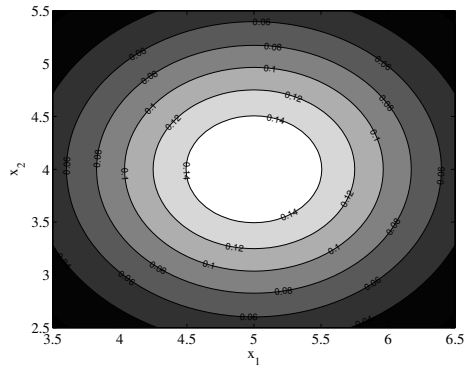

(a) Initial pdf in cartesian variables

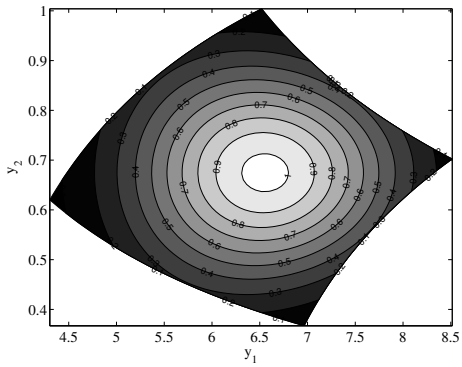

(b) Mapped pdf in polar variables

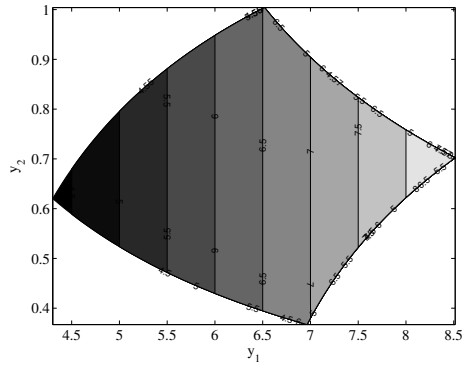

(c) Contour levels of $1 \Big/ \mathcal{T}_{\left|\det \frac{\partial \boldsymbol{f}}{\partial \boldsymbol{x}}\right|}(\boldsymbol{x})$

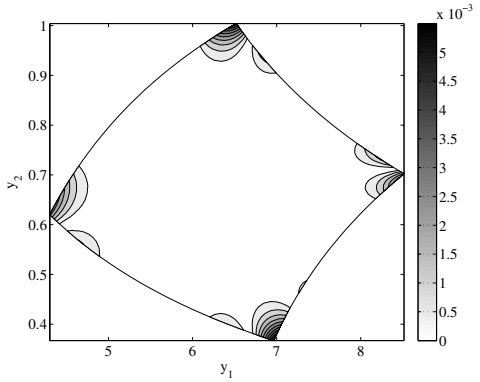

(d) Relative error of $1 \Big/ \mathcal{T}_{\left|\det \frac{\partial \boldsymbol{f}}{\partial \boldsymbol{x}}\right|}(\boldsymbol{x})$

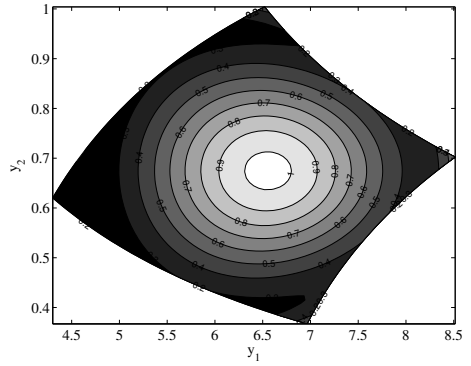

(e) Mapped pdf with the partial DA method

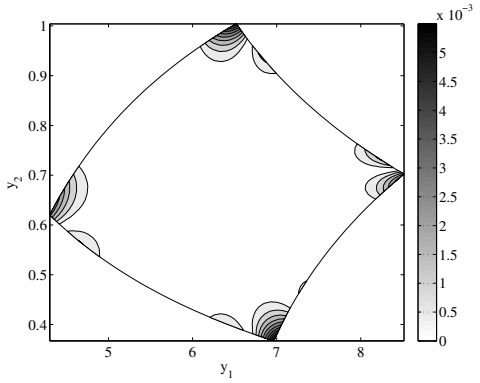

(f) Relative error of the partial DA method (percentage)

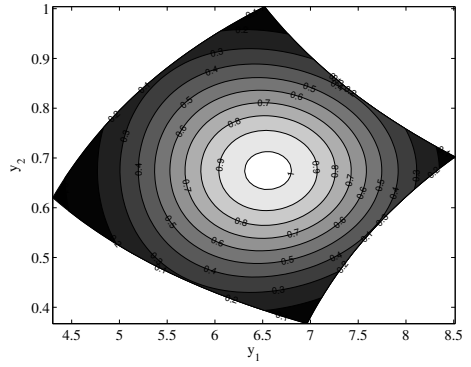

(g) Mapped pdf with the full DA method

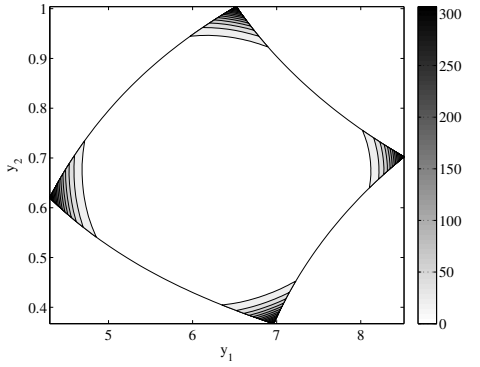

(h) Relative error of the full DA method (percentage)

Figure 1: Pdf mapping for the cartesian to polar transformation: analytic solutions vs. Taylor approximation.

Table 1: Test cases: orbital parameters

Test Case		A	B
Orbit type		GEO	LEO
SSC		26824	04784
Epoch	JED	2457163.2824	2457155.9737
a	km	42143.781	7353.500
e	–	0.000226	0.002640
i	deg	0.0356	74.0295
Ω	deg	26.278	179.640
ω	deg	42.052	359.079
M	deg	72.455	99.458

tory, Canary Islands). The observations are separated by 12 min (approximately by an arc lenght of 3 deg). A resolution of $\sigma_{\alpha,\delta} = 0.5$ arcsec is considered for both the right ascension and declination.

For the LEO case two radar observations taken with the Chilbolton Advanced Meteorological Radar (CAMRa, Chilbolton Observatory, UK) are simulated. The observations are separated by 2 minutes, approximately an arc length of 7 deg, such that the range from the station remains of the order of 1000 km. The range has a resolution of $\sigma_\rho = 25$ m, and the pointing angles have standard deviations $\sigma_{\alpha,\delta} = 0.25$ deg.

Test Case A

Figure 2 shows the results of the pdf mapped from the observation space into the modified equinoctial elements space $\boldsymbol{y}_{MEE} = (p, f, g, h, k, L)$, in which $p = a(1-e^2)$ is the semilatus rectum, $f = e\cos(\omega+\Omega)$ and $g = e\sin(\omega+\Omega)$, $h = \tan(i/2)\cos(\Omega)$ and $k = \tan(i/2)\sin(\Omega)$, and the true longitude $L = \Omega+\omega+\nu$. The set $\boldsymbol{y}_{COE} = (a, e, i, \Omega, \omega, \nu)$ represents the classical orbital elements. The plots are obtained by processing 100,000 normally distributed vectors generated in the observation space using the MATLAB function mvnrnd. Each sample is mapped from the observation space $(\boldsymbol{\alpha}, \boldsymbol{\delta})$ into the state space $\boldsymbol{y}_{MEE}$ at the epoch of the second observation by using the Taylor approximation $\boldsymbol{y}_{MEE} = \mathcal{T}_{\boldsymbol{y}_{MEE}}(\boldsymbol{\alpha}, \boldsymbol{\delta})$. The probability of each mapped sample is obtained by multiplying its probability $p(\boldsymbol{\alpha}, \boldsymbol{\delta})$ by the Taylor representation of the inverse of the determinant of the Jacobian of the O2S map, i.e. $p(\boldsymbol{y}_{MEE}) = p(\mathcal{T}_{\boldsymbol{y}_{MEE}}(\boldsymbol{\alpha}, \boldsymbol{\delta})) = p(\boldsymbol{\alpha}, \boldsymbol{\delta})\ 1/\left|\mathcal{T}_{\frac{\partial \boldsymbol{y}_{MEE}}{\partial(\boldsymbol{\alpha},\boldsymbol{\delta})}}\right|$. The obtained probability values are then scaled in the range $[0, 1]$ for a better readability of the plots.

Figure 2 shows that, although the size of the uncertainty map is large, the mapped pdf still (visually) resembles a Gaussian distribution. The uncertainty set is large as the optical observations are taken on a short arc, and thus the sensitivity of the solution to uncertainties in the measurements is high. In addition, in a short arc, the nonlinearities of the dynamics do not play a significant role and thus the pdf remains nearly Gaussian. This qualitative argument is supported by comparing the covariance matrices computed with samples mapped with 6th and 1st order expansions, as reported in Table 2 and 3. The difference between the two matrices in all the components is less than 1%.

However it is important to notice that the selection of MEE is particularly suited to maintain the

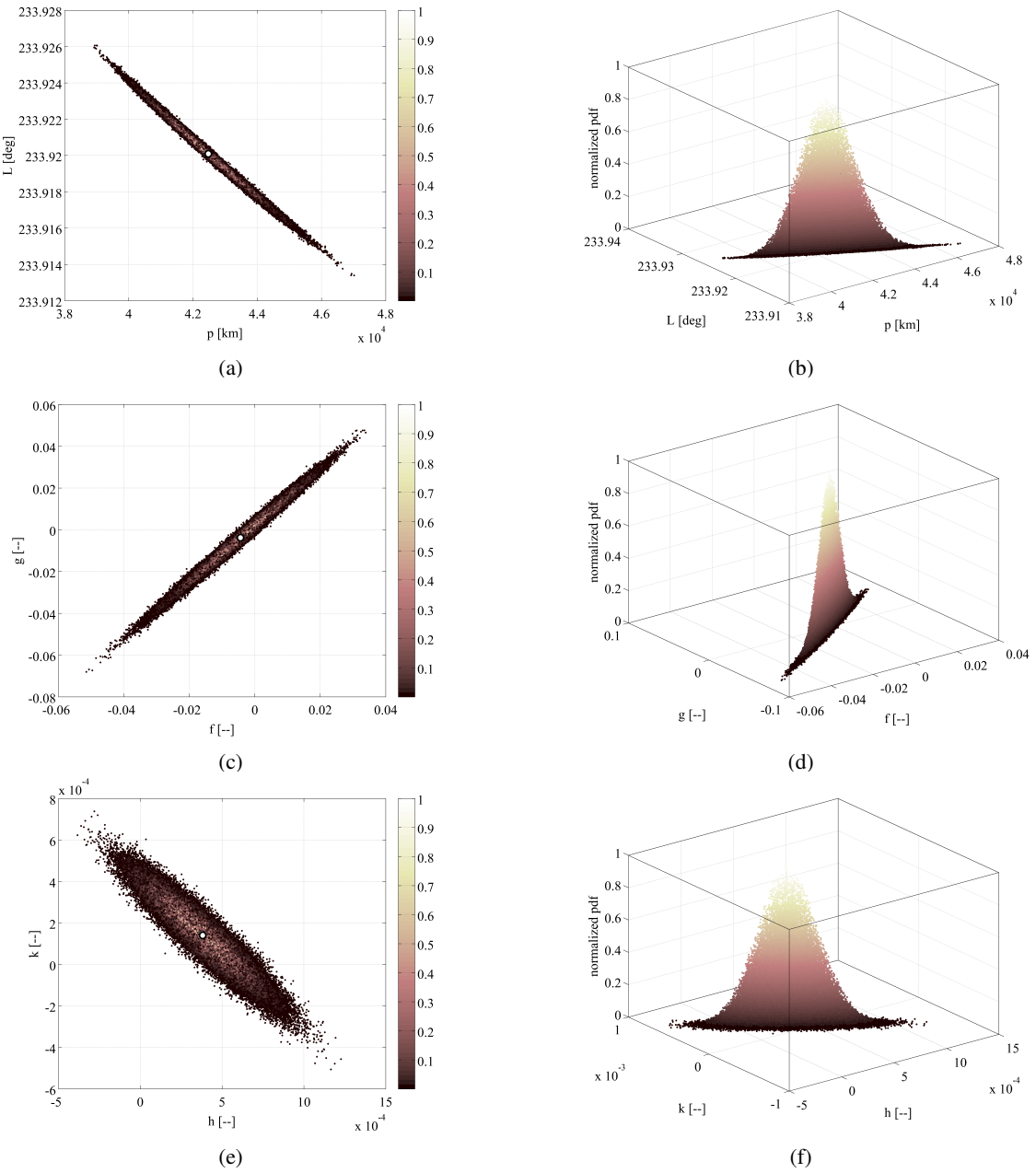

Figure 2: Mapped pdf in the MEE space for optical observations

p [km]	f	g	h	k	L [rad]
8.816e+05	-9.276e+00	-1.270e+01	1.777e-01	-1.276e-01	-2.470e-02
-9.276e+00	9.817e-05	1.333e-04	-1.887e-06	1.319e-06	2.587e-07
-1.270e+01	1.333e-04	1.833e-04	-2.548e-06	1.855e-06	3.569e-07
1.777e-01	-1.887e-06	-2.548e-06	3.641e-08	-2.492e-08	-4.942e-09
-1.276e-01	1.319e-06	1.855e-06	-2.492e-08	1.956e-08	3.628e-09
-2.470e-02	2.587e-07	3.569e-07	-4.942e-09	3.628e-09	6.967e-10

Table 2: Covariance matrix in MEE computed with samples mapped at 6th order: test case A

p [km]	f	g	h	k	L [rad]
8.773e+05	-9.236e+00	-1.265e+01	1.772e-01	-1.272e-01	-2.463e-02
-9.236e+00	9.779e-05	1.327e-04	-1.882e-06	1.316e-06	2.581e-07
-1.265e+01	1.327e-04	1.826e-04	-2.542e-06	1.851e-06	3.560e-07
1.772e-01	-1.882e-06	-2.542e-06	3.637e-08	-2.489e-08	-4.936e-09
-1.272e-01	1.316e-06	1.851e-06	-2.489e-08	1.954e-08	3.624e-09
-2.463e-02	2.581e-07	3.560e-07	-4.936e-09	3.624e-09	6.960e-10

Table 3: Covariance matrix in MEE computed with samples mapped at 1st order: test case A

normality of the statistics. The impact of orbital elements selection on the mapped pdf is shown in Figure 3 and in the normality plots of Figure 5. As the orbital eccentricity cannot take negative values, the mapped pdf is clearly not Gaussian when classical orbital elements are used (see Figure 3). As shown in Figure 5(f) also the true anomaly is not normally distributed. This is due to both the low eccentricity and inclination of the test orbit: a small variation in the observations can produce a large variation in all the true anomaly, the pericenter anomaly and the right ascension of the node; whereas the true longitude (the sum of these three angles) is significantly less affected.

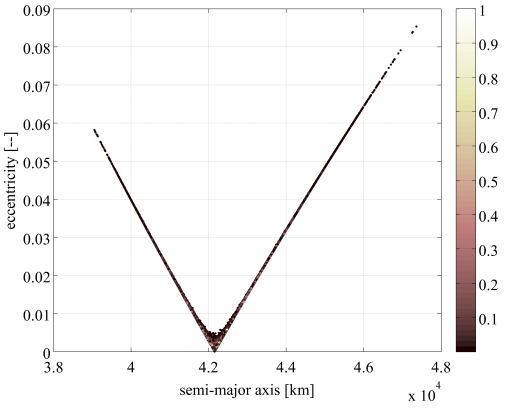

Figure 3: Samples projections in the semi-major axis and eccentricity space

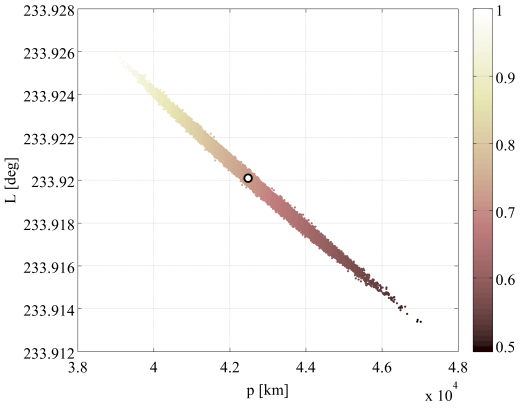

Figure 4: Mapped pdf in classical orbital elements and for uniform initial distribution

The proposed approach for mapping pdfs is independent from the initial pdf and can be used to

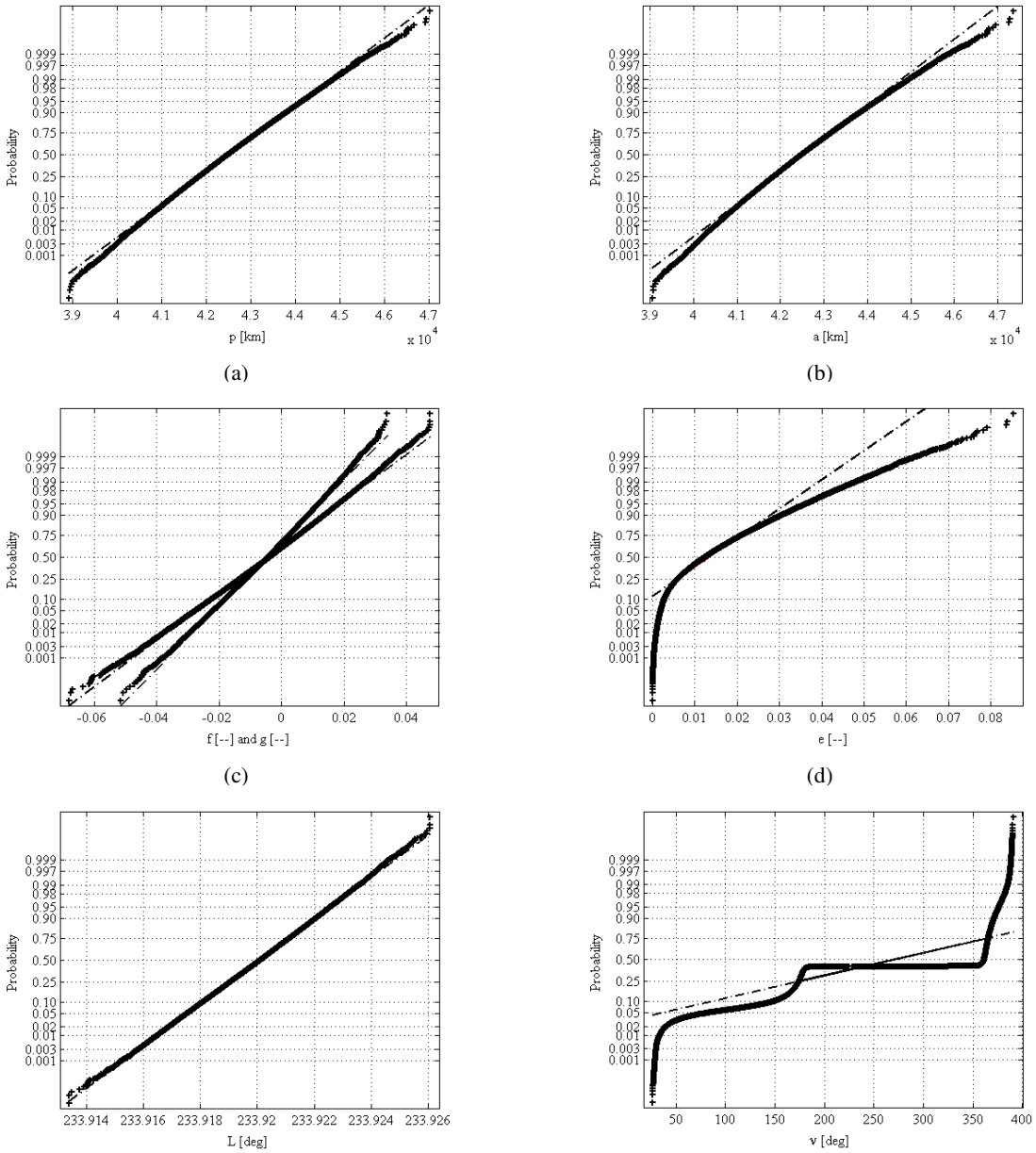

Figure 5: Normality plots: comparison between MEE (left) and COE (right). The dashed lines are extensions of the line connecting the 25th and 75th percentiles of the distribution: proximity of the distributions to the dashed lines indicates validity of the normality assumption.

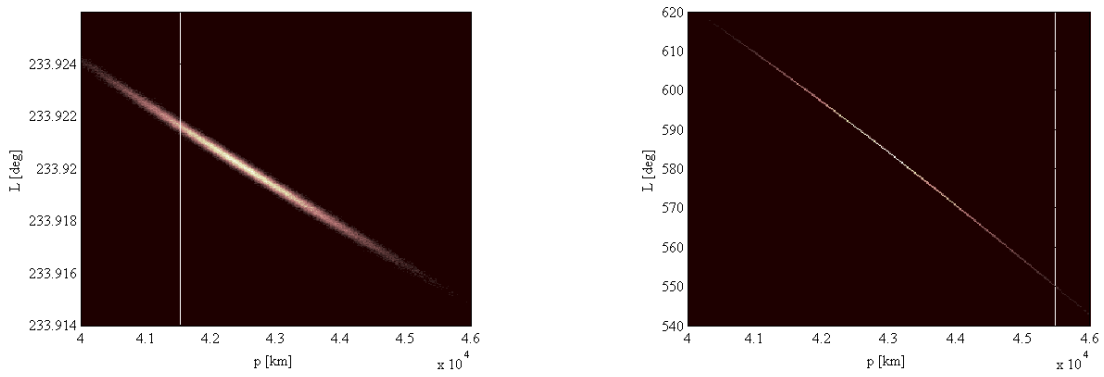

(a) Epoch t_2

(b) Epoch t_2+ 1 day

Figure 6: Samples binned in the true longitude and semilatus rectum space

error	α_1 [arcsec]	δ_1 [arcsec]	α_2 [arcsec]	δ_2 [arcsec]	α_3 [arcsec]	δ_3 [arcsec]
mean	1.209e-06	6.935e-06	9.821e-08	7.374e-06	1.018e-06	7.817e-06
mad	1.924e-06	8.558e-06	1.546e-07	9.076e-06	1.623e-06	9.601e-06
max	6.852e-04	1.253e-03	5.504e-05	1.361e-03	5.750e-04	1.465e-03

Table 4: Error on observables for 6th order computations: test case A

map a pdf to any arbitrary time. Figure 4 illustrates an example when a uniform distribution of the observation errors is assumed in the 6th dimensional cube of side $[-3\sigma_{\alpha,\delta}, 3\sigma_{\alpha,\delta}]$. In this particular case, the mapped pdf depends only on the determinant of the Jacobian of the transformation. In Figure 6 the 100,000 normal distributed samples are binned in the space of the semilatus rectum and true longitude. On the left side the bins are plotted at the time of the second observation t_2, whereas on the right side a 6th order expansion of the flow of the Keplerian dynamics is used to map them ahead for 1 day. It is apparent how the dynamics stretches the set along the orbit. After approximately 1 revolution the set is spread on an arc length of more than 50 deg.

The proposed approach is valid as long as the Taylor approximation of the transformation is accurate enough. In order to verify the accuracy of the expansion of the O2S map, for each sample generated in the observation space, we evaluate the associated state in MEE and then compute the predicted observations. The accuracy of the expansion is assessed by a statistical analysis of the difference between the observed (i.e. sampled) and predicted observations. Table 4 shows the results when 6th order computations are carried out. It is clear that the mean, maximum absolute deviation (mad), and the maximum (max) errors are all orders of magnitude lower than the measurements errors. This proves that a 6th order expansion accurately approximate the O2S map. This accuracy degrades when lower expansion orders are adopted. Indeed, Table 5 shows that the errors at first order are grater than the measurement uncertainties.

Test case B

The results obtained for the radar observations are plotted in the same way as in test case A, using always 100,000 normally distributed samples. Figure 7 shows the samples as well as their proba-

error	α_1 [arcsec]	δ_1 [arcsec]	α_2 [arcsec]	δ_2 [arcsec]	α_3 [arcsec]	δ_3 [arcsec]
mean	1.378e+00	2.558e+00	1.463e-01	2.550e+00	1.085e+00	2.563e+00
mad	1.332e+00	2.474e+00	1.415e-01	2.465e+00	1.049e+00	2.478e+00
max	2.470e+01	4.523e+01	2.591e+00	4.509e+01	1.953e+01	4.534e+01

Table 5: Error on observables for first order computations: test case A

p [km]	f	g	h	k	L [rad]
7.7549e+03	-6.7877e-01	-8.3243e-01	-8.3099e-02	-1.0538e-01	6.2044e-02
-6.7877e-01	6.4034e-05	6.9527e-05	4.5889e-06	5.7960e-06	-1.3238e-06
-8.3243e-01	6.9527e-05	9.1760e-05	1.0830e-05	1.3735e-05	-9.5763e-06
-8.3099e-02	4.5889e-06	1.0830e-05	6.6146e-06	9.4941e-06	-9.0577e-06
-1.0538e-01	5.7960e-06	1.3735e-05	9.4941e-06	1.3819e-05	-1.3170e-05
6.2044e-02	-1.3238e-06	-9.5763e-06	-9.0577e-06	-1.3170e-05	1.2896e-05

Table 6: Covariance matrix in MEE computed with samples mapped at 6th order: test case B.

bility, scaled in the range $[0, 1]$. In this case the large uncertainties associated with the instrument pointing angles result in a large uncertainty set in the MEE space. Nevertheless, the normality distribution of the samples is preserved due to the short temporal separation between the observations. This is clearly highlighted by the covariance matrices of the MEE samples obtained with computations at 6th and first order, as reported in Table 6 and 7. Nevertheless, the 6th order expansion is significantly more accurate in representing the O2S map, as shown by the error analysis of Table 8 and 9. Note that in the first order approximation the maximum errors on the computed observations are of the same order of magnitude of the measurement accuracies.

As for the optical case, the selection of the set of orbital parameters used for the representation of the spacecraft state plays a key role on the characteristics of the mapped pdf. Figure 8 confirms that, when COE are used, the samples are no longer normally distributed in eccentricity, as this orbital parameter cannot take negative values.

As already mentioned in Section *Two position vectors IOD*, given the two position vectors and the elapsed time between the observations in the radar observations scenario, we solve a Lambert's problem to compute the Taylor approximation of the velocity vectors at the end points using DA.

p [km]	f	g	h	k	L [rad]
7.7547e+03	-6.7881e-01	-8.3237e-01	-8.3119e-02	-1.0540e-01	6.2068e-02
-6.7881e-01	6.4040e-05	6.9530e-05	4.5902e-06	5.7976e-06	-1.3250e-06
-8.3237e-01	6.9530e-05	9.1749e-05	1.0833e-05	1.3738e-05	-9.5794e-06
-8.3119e-02	4.5902e-06	1.0833e-05	6.6142e-06	9.4939e-06	-9.0573e-06
-1.0540e-01	5.7976e-06	1.3738e-05	9.4939e-06	1.3818e-05	-1.3169e-05
6.2068e-02	-1.3250e-06	-9.5794e-06	-9.0573e-06	-1.3169e-05	1.2895e-05

Table 7: Covariance matrix in MEE computed with samples mapped at first order: test case B.

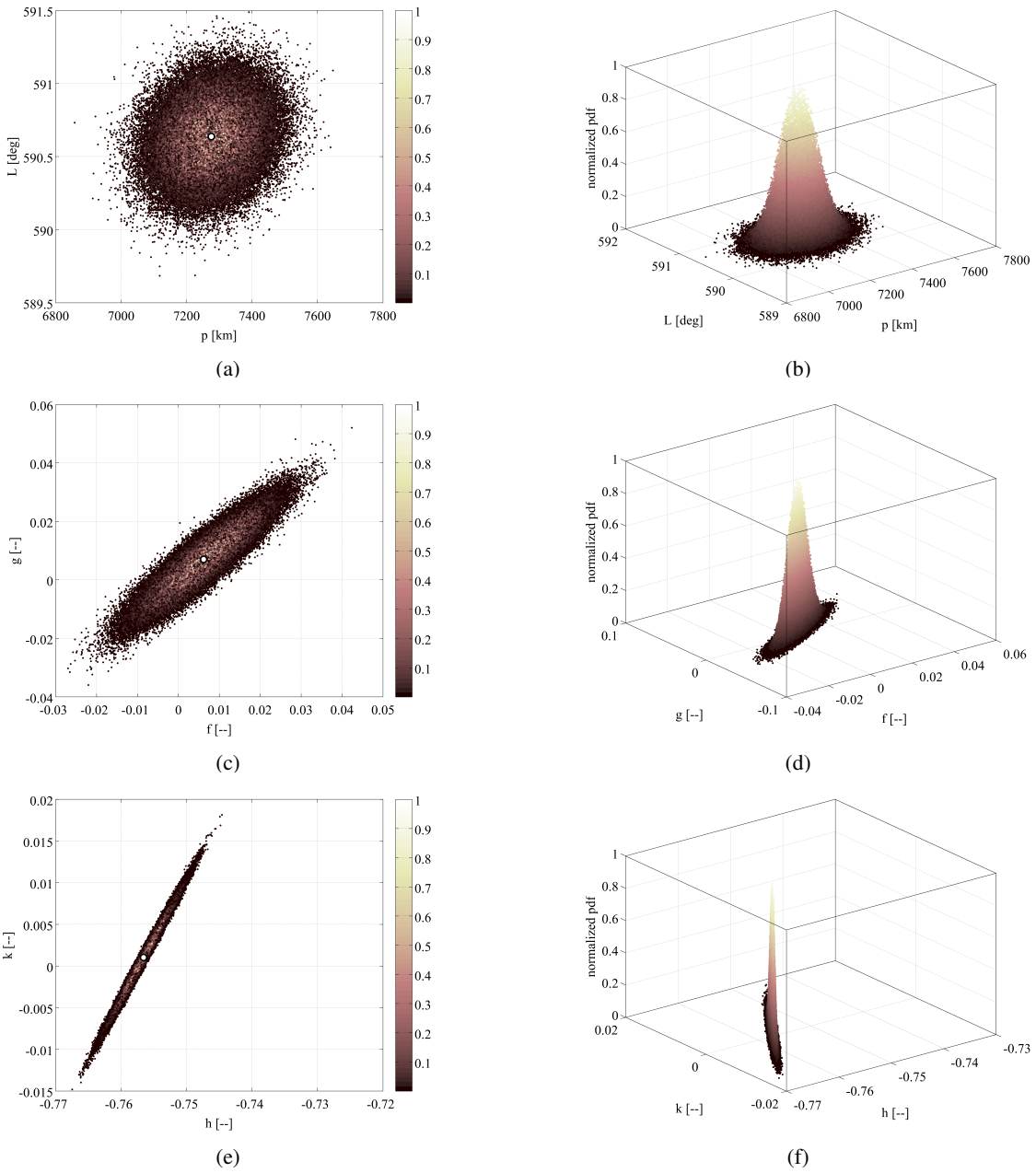

Figure 7: Mapped pdf in the MEE space for radar observations

error	ρ_1 [km]	α_1 [arcsec]	δ_1 [arcsec]	ρ_2 [km]	α_2 [arcsec]	δ_2 [arcsec]
mean	4.5830e-09	3.8504e-06	4.2332e-07	7.0521e-10	1.0749e-05	4.2037e-07
mad	6.2071e-09	5.3498e-06	5.8808e-07	8.8516e-10	1.4942e-05	5.8187e-07
max	3.8123e-06	3.5275e-03	3.0735e-04	5.8235e-07	9.2682e-03	5.4619e-04

Table 8: Error on observables for 6th order computations: test case B.

error	ρ_1 [km]	α_1 [arcsec]	δ_1 [arcsec]	ρ_2 [km]	α_2 [arcsec]	δ_2 [arcsec]
mean	5.5931e-02	1.5414e+01	9.2369e+00	5.0393e-02	3.9147e+01	1.4969e+01
mad	4.5940e-02	1.5053e+01	8.4973e+00	4.0140e-02	3.4114e+01	1.4327e+01
max	1.4028e+00	4.4737e+02	2.1175e+02	7.5218e-01	9.0253e+02	4.4621e+02

Table 9: Error on observables for first order computations: test case B.

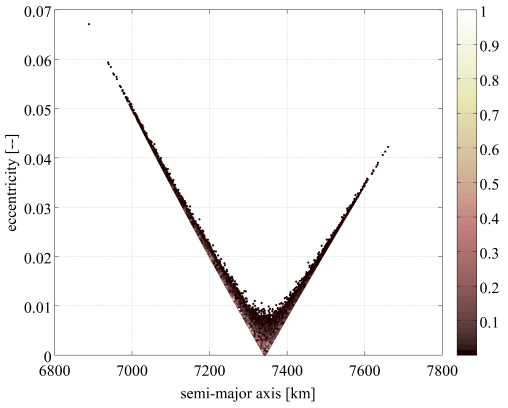

Figure 8: Samples projections in the semi-major axis and eccentricity space

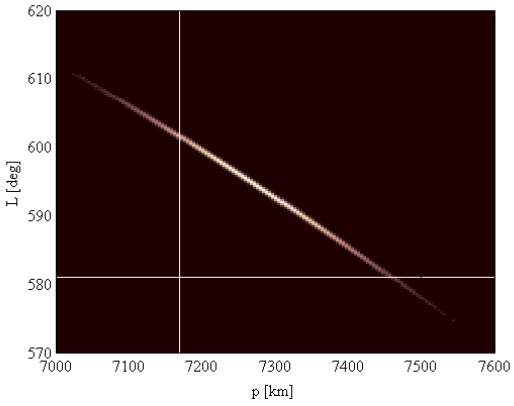

Figure 9: Samples binned in the true longitude and semilatus rectum space after one orbital revolution propagated with AIDA

The solution of the Lambert's problem relies on the assumption of a Keplerian motion. Nevertheless, the proposed method can be easily extended to apply to more complex dynamics. The Lambert's problem is replaced by the two-point boundary value problem (TPBVP) of linking two position vectors in a given elapsed time in general dynamics. An approach to compute the Taylor expansion of TPBVPs in any dynamics using DA was presented in Di Lizia et al.[23] Thus, the same approach is used here to solve the IOD problem by predicting the motion of the object using the numerical propagator AIDA (Accurate Integrator for Debris Analysis[?]), which includes geopotential acceleration, atmospheric drag, solar radiation pressure, and third body gravity as perturbations to the Keplerian motion. All the remaining steps of the proposed method remain unchanged.

Table 10 compares the mean MEEs at epoch t_1 of the first observation obtained using Kepler's dynamics with the MEEs at the same epoch computed with AIDA. Due to the short time between the two observations, the effect of the perturbations introduced with AIDA is negligible. This is confirmed by comparing the covariance matrices of the MEE samples obtained with 6th order computations in Keplerian dynamics (Table 6) and with AIDA (Table 11).

Similarly to test case A, the proposed method is used to map the pdf of the MEE from epoch t_1 to epoch $t_1 + T$, in which T is the period of the nominal solution. Unlike the previous case, to investigate the long-term effects of perturbations and show the versatility of the proposed method, the pdf is mapped at $t_1 + T$ by a 6th order expansion of the flow computed with AIDA. The result is shown in Figure 9 by binning the resulting samples. Once again, the dynamics stretches the set along the orbit and, after one revolution, the set is spread on an arc length of about 30 deg. As a clear effect of the increasing nonlinearities, the set starts bending, so drifting apart from the normal

	p [km]	f	g	h	k	L [rad]
Kepler	7.276e+03	6.152e-03	6.995e-03	-7.566e-01	1.015e-03	1.031e+01
AIDA	7.275e+03	6.109e-03	7.071e-03	-7.566e-01	9.304e-04	1.031e+01

Table 10: Comparison of mean MEE computed with Keplerian dynamics and AIDA propagator

p [km]	f	g	h	k	L [rad]
7.7938e+03	-6.7748e-01	-8.3909e-01	-8.4680e-02	-1.0835e-01	6.4515e-02
-6.7748e-01	6.3303e-05	6.9782e-05	4.8118e-06	6.1639e-06	-1.6860e-06
-8.3909e-01	6.9782e-05	9.2597e-05	1.0894e-05	1.3914e-05	-9.6762e-06
-8.4680e-02	4.8118e-06	1.0894e-05	6.6848e-06	9.6409e-06	-9.1776e-06
-1.0835e-01	6.1639e-06	1.3914e-05	9.6409e-06	1.4094e-05	-1.3403e-05
6.4515e-02	-1.6860e-06	-9.6762e-06	-9.1776e-06	-1.3403e-05	1.3092e-05

Table 11: Covariance matrix in MEE computed with samples mapped at 6th order: test case B with AIDA propagator

distribution.

CONCLUSIONS

A general method for mapping a pdf from the observations space into object state space in an IOD process has been presented. This method is based on the high order Taylor expansion of both the O2S map and its Jacobian. A simple cartesian to polar transformation has been used as illustrative example to show the method performance in a test case with an available analytical solution. Then, the approach has been tested on two IOD scenarios, an optical observation of a spacecraft in GEO and a radar observation of a spent rocket in LEO. It has been shown that DA can be effectively used to nonlinearly map pdf, and that the method is independent of the model used to describe the spacecraft dynamics as well as of the pdf of the measurements.

ACKNOWLEDGMENTS

R. Armellin acknowledges the support received by the Marie Sklodowska-Curie grant 627111 (HOPT - Merging Lie perturbation theory and Taylor Differential algebra to address space debris challenges). This work has been partially funded by the Spanish Finance and Competitiveness Ministry under Project ESP2014-57071-R.

REFERENCES

[1] P. W. Schumacher, C. Sabol, C. C. Higginson, and K. T. Alfriend, "Uncertain Lambert Problem," *Journal of Guidance, Control, and Dynamics*, 2015, pp. 1–12, 10.2514/1.G001019.

[2] C. F. Gauss, *Theoria Motus Corporum Coelestium in Sectionibus Conicis Solem Ambientium*. sumtibus Frid. Perthes et IH Besser, 1809.

[3] P. Laplace, "Mémoires de l'Académie Royale des Sciences," *Paris, Reprinted in Laplace's Collected Works*, Vol. 10, 1780.

[4] G. Merton, "A modification of Gauss's method for the determination of orbits," *Monthly Notices of the Royal Astronomical Society*, Vol. 85, 1925, p. 693.

[5] A. Celletti and G. Pinzari, "Dependence on the observational time intervals and domain of convergence of orbital determination methods," *Periodic, Quasi-Periodic and Chaotic Motions in Celestial Mechanics: Theory and Applications*, pp. 327–344, Springer, 2006.

[6] G. F. Gronchi, "Multiple solutions in preliminary orbit determination from three observations," *Celestial Mechanics and Dynamical Astronomy*, Vol. 103, No. 4, 2009, pp. 301–326.

[7] P. R. Escobal, "Methods of orbit determination," *New York: Wiley, 1965*, Vol. 1, 1965.

[8] R. Gooding, "A new procedure for the solution of the classical problem of minimal orbit determination from three lines of sight," *Celestial Mechanics and Dynamical Astronomy*, Vol. 66, No. 4, 1996, pp. 387–423.

[9] R. Battin, *An Introduction to the Mathematics and Methods of Astrodynamics*. Reston, VA: AIAA Education Series, 1999.

[10] R. Gooding, "A procedure for the solution of Lambert's orbital boundary-value problem," *Celestial Mechanics and Dynamical Astronomy*, Vol. 48, No. 2, 1990, pp. 145–165.

[11] N. Arora and R. Russell, "A fast and robust multiple revolution Lambert algorithm using a cosine transformation," *Paper AAS*, Vol. 13-728, 2013.

[12] K. Muinonen and E. Bowell, "Asteroid orbit determination using Bayesian probabilities," *Icarus*, Vol. 104, No. 2, 1993, pp. 255–279.

[13] J. Virtanen, K. Muinonen, and E. Bowell, "Statistical ranging of asteroid orbits," *Icarus*, Vol. 154, No. 2, 2001, pp. 412–431.

[14] C. R. Binz and L. M. Healy, "Uncertainty Characterization for Angles-Only Initial Orbit Determination," *Advances in the Astronautical Sciences*, Vol. 150, 2014, pp. 1777–1792.

[15] C. W. Roscoe, I. I. Hussein, P. W. Schumacher Jr, and M. P. Wilkins, "On Uncertain Angles-Only Track Initiation for SSA," *AIAA/AAS Astrodynamics Specialist Conference*, 2014, p. 4468.

[16] M. Berz, *Differential Algebraic Techniques, Entry in Handbook of Accelerator Physics and Engineering*. New York: World Scientific, 1999a.

[17] T. Soong, *FUNDAMENTALS OF PROBABILITY AND STATISTICS FOR ENGINEERS*, Vol. 50. John Wiley & Sons, 2004, 10.2307/2684940.

[18] A. Wittig, C. Colombo, and R. Armellin, "Density of high area-to-mass objects in geostationary and medium Earth orbits through semi-analytical equations and differential algebra," *International Astronautical Congress, IAC 2014. Proceedings of the*, IAF, 2014, pp. 1–11.

[19] M. Berz, *The new method of TPSA algebra for the description of beam dynamics to high orders*. Los Alamos National Laboratory, 1986. Technical Report AT-6:ATN-86-16.

[20] M. Berz, "The method of power series tracking for the mathematical description of beam dynamics," *Nuclear Instruments and Methods A258*, 1987.

[21] M. Berz, *Modern Map Methods in Particle Beam Physics*. Academic Press, 1999b.

[22] M. Berz and K. Makino, *COSY INFINITY version 9 reference manual*. Michigan State University, East Lansing, MI 48824, 2006. MSU Report MSUHEP060803.

[23] P. Di Lizia, R. Armellin, and M. Lavagna, "Application of high order expansions of two-point boundary value problems to astrodynamics," *Celestial Mechanics and Dynamical Astronomy*, Vol. 102, No. 4, 2008, pp. 355–375.

[24] R. Armellin, P. Di Lizia, and M. Lavagna, "High-order expansion of the solution of preliminary orbit determination problem," *Celestial Mechanics and Dynamical Astronomy*, Vol. 112, No. 3, 2012, pp. 331–352.

[25] A. Wittig, P. Di Lizia, R. Armellin, K. Makino, F. Bernelli-Zazzera, and M. Berz, "Propagation of large uncertainty sets in orbital dynamics by automatic domain splitting," *Celestial Mechanics and Dynamical Astronomy*, Vol. 122, No. 3, 2015, pp. 239–261.

[26] R. Armellin, P. Di Lizia, F. Topputo, M. Lavagna, F. Bernelli-Zazzera, and M. Berz, "Gravity assist space pruning based on differential algebra," *Celestial mechanics and dynamical astronomy*, Vol. 106, No. 1, 2010, pp. 1–24.